Optimizing Large Scale Imaging Surveys for Relative Photometric Calibration

R. Holmes[1] and H.-W. Rix[1]

Max-Planck-Institut für Astronomie, Königstuhl 17, Heidelberg, 69117, Germany.

and

D. W. Hogg[2]

2 Center for Cosmology and Particle Physics, Department of Physics, New York University,

4 Washington Place, New York, NY 10003, USA.

Received ______________________; accepted ______________________

ABSTRACT

In this paper we show that, with due care given to the observing strategy, it will be possible to accurately constrain the relative photometric calibration of instruments used in large imaging surveys with their science data alone. We create end-to-end simulations of an imaging survey, which produces simulated datasets from mock observations of a synthetic sky according to a defined survey strategy. These catalog based simulations include realistic measurement uncertainties and a complex, position dependent instrument response. We then use a self-calibration technique to recover the relative instrument response by fitting an model that best explains the survey dataset, based on the multiple observations of (non-varying) sources at different focal plane positions. By considering four simple survey strategies we find that, with a correct redundancy built into the survey strategy, it is possible to accurately constrain the relative photometric response of an imaging instrument, and therefore the relative calibration of the resulting dataset. The majority of the remaining post self-calibration errors are due to the limitations in the basis used to model the relative instrument response. We find that returning the same sources to very different focal plane positions is the key property of a survey strategy that is required for an accurate calibration. From the results of this work, we are able to highlight an important point for those considering the design of large scale imaging surveys: depart from a regular tiling of the sky and return the same sources to very different focal plane positions.

Subject headings: Relative Photometric Calibration: Imaging Survey: Euclid

1. Introduction

Astronomers tend to think in terms of taking science data and calibration data separately. The former is used for science and the latter is used to constrain instrument parameters like the flat-field, the dark currents and so-on. But typically far more photons are collected during science exposures; are these not incredibly constraining on the calibration themselves? Indeed, in the retrospective photometric calibration of the Sloan Digital Sky Survey data (SDSS) much more calibration information was obtained from the science data than the calibration data (Padmanabhan et al. 2008). But, of course, the SDSS imaging strategy had to be adjusted to make this calibration work: good redundancy is required in the data stream, and a redundancy of a very specific kind.

In this paper, we argue that the next generation of large surveys should have their observation strategies optimized from the very start with this "self-calibration" in mind. We focus here on the relative photometric calibration of a typical imaging instrument only, although we also suspect that similar techniques could be used to constrain many other calibration parameters. This technique utilizes the multiple measurements of (non-varying) sources at different focal plane positions and at different times within the survey to constrain the relative instrument response by requiring that they yield the same count values. Through end-to-end – catalog level – survey simulations[1], we aim to identify the important properties of survey strategies that makes them advantageous for this kind of self-calibration.

These simulations include a complex, position dependent instrument response; through mock observations of a synthetic sky, according to a defined survey strategy, we construct a realistic survey dataset. We then fit a (different) instrument response model that best

[1]All of the code used in this work is publicly available at XX.

describes this dataset. By comparing the *fitted* instrument response to the *true* instrument response we are able to assess the performance of the self-calibration procedure with different survey strategies. There is a degeneracy in this problem: the self-calibration procedure is only able to fit for a *relative* instrument response. We have no way of know, for example, if all the sources are uniformly fainter, or if the instrument sensitivity is uniformly lower.

In Section 2 we introduce the simulation chain constructed to produce the realistic survey datasets. Section 3 goes onto to detail the self-calibration procedure. In Section 5 we focus on four simple survey strategies, which allow us to draw conclusions on the performance of the self-calibration procedure with different survey properties. We do not produced pixelated images; instead we concentrate on catalog level simulations with realistic measurement uncertainties. Complex effects are included in the simulations that are not precisely modeled at the analysis stage, in order to simulate the effects of unknown systematic errors within the dataset.

2. Survey Dataset Simulations

We have constructed an end-to-end simulation chain that produces a realistic imaging dataset from a specified survey strategy. Simulation parameters are kept intentionally flexible, so that the sensitivity of the self-calibration procedure to different parameters can be investigated. The simulations are split into a number of steps. First, a synthetic sky is generated based on the specified simulation parameters (density of sources, magnitude ranges). With a given pointing, single mock observations are performed on this sky, again here with tunable simulation parameters, such as the instrument response model and the the noise model. The final step is the build up of the survey wide dataset from multiple single observations taken according to the prescribed survey strategy. In this section, we detail the assumptions and methods used in each of these steps.

2.1. The Synthetic Sky

We generate a representative synthetic sky based on realistic object densities in the AB magnitude range $m_{\rm min} = 17$ to $m_{\rm max} = 22$ mag$_{\rm AB}$, with these limits chosen to be consistent with the saturation and 10σ limits of deep, space-based, near-infrared survey. Sources are generated with random coordinates (uniformly distributed within the sky region being investigated) and with random magnitudes m distributed according to

$$\log_{10} \frac{\mathrm{d}N}{\mathrm{d}m\,\mathrm{d}\Omega} = a + b\,m + c\,m^2 \quad , \tag{1}$$

where $\frac{\mathrm{d}N}{\mathrm{d}m\,\mathrm{d}\Omega}$ is the density of sources N per unit magnitude m and per unit solid angle Ω, and a, b and c are model parameters. Even though our simulations make no distinction between galaxies and stars, the values of the parameters are found from fitting the Y-band galaxy populations reported in Windhorst et al. (2011) (Windhorst et al. 2011) only. These parameters were $a = -13.05$, $b = 1.25$ and $c = -0.02$. We intentionally omit the stellar population, so that the conclusions drawn from these simulations are independent of the final position of the survey area on the sky. The source magnitudes m are related to the source fluxes s simply by: $m = 22.5 - 2.5\log_{10}(s)$, where the 22.5 puts the fluxes in units of nanomaggies (nmgy). Due to computational reasons, we only select the brightest sources within the survey area, up to a source density d, for the self-calibration procedure.

2.2. A Single Exposure

With a camera pointing (α, β) and camera orientation θ this synthetic sky is transformed into focal plane coordinates and all of the sources falling within the instrument's field-of-view are found. In our simulations, we use a large instrument field-of-view of 0.76 deg $\times$ 0.72 deg;

a size consistent with the next generation of large survey imagers. An example of a single pointing exposure is shown in Figure 1.

2.2.1. Measured Count Rates

We do not consider pixelated images in these simulations; instead the true source fluxes $s_{\rm true}$ are converted into measured count rates c with an complex, position dependent instrument response model $f_{\rm true}$ and a measurement noise model. For a measurement i the count rate c_i recorded from a source k depends on the *true* instrument response $f_{\rm true}(\vec{x_i}|\vec{q}_{\rm true})$, which is a function of focal plane position $\vec{x_i}$, and the source's true flux $s_{k,{\rm true}}$

$$c_i = f_{\rm true}(\vec{x_i}|\vec{q}_{\rm true})\, s_{k,{\rm true}} + e_i \quad ,$$

where $\vec{q}_{\rm true}$ are the parameters defining the *true* instrument response, and e_i is a noise contribution drawn from the Normal Distribution $N(e|0, {\sigma_{\rm true}}^2)$.

2.2.2. Noise Model

To construct the noise model, the simulated exposures are assumed to be background limited and that, for systematic reasons, there is an upper limit on the signal-to-noise ratio of 500 for bright sources. The noise model is complicated further by applying an extra term ϵ_i to the count rates' uncertainty variance, which we intentionally do not take into account in the analysis in order to simulate systematic problems with the instrument noise model. The *true* noise model is therefore

$$\sigma_{i,{\rm true}}^2 = (1+\epsilon_i)\,\alpha^2 + \eta^2\left[f_{\rm true}(\vec{x_i}|\vec{q}_{\rm true})\, s_{k,{\rm true}}\right]^2 \quad , \tag{2}$$

where α and η are both constants and ϵ_i is a random number, in the range $[0.0,\, \epsilon_{max})$, generated for each measurement i. The $m = 22$ mag 10σ detection limit introduced previously and the 500 limit on the signal-to-noise ratio are used to set $\alpha = 0.1585$ and $\eta = 0.0017$. The ϵ_i contribution is not taken into account in the analysis stage and therefore the uncertainty variances on the count rates are assumed to be

$$\sigma_i^2 = \alpha^2 + \eta^2\, c_i^2$$

during the analysis stage.

2.2.3. The True Instrument Response Model

We construct a complex, position independent instrument response model $f_{\rm true}(\vec{x_i}|\vec{q}_{\rm true})$ from a superposition of large and small-scale variations:

$$f_{\rm true}(\vec{x_i}|\vec{q}_{\rm true,1...260}) = f_{\rm large}(\vec{x_i}|\vec{q}_{\rm true,1...6}) + f_{\rm small}(\vec{x_i}|\vec{q}_{\rm true,7...260}) \quad ,$$

where $\vec{x_i} = (x_i, y_i)$ is the focal plane position that the kth source falls at during the $i^{\rm th}$ measurement and $\vec{q}_{\rm true}$ are the parameters defining the instrument response model. The large-scale instrument response $f_{\rm large}(\vec{x_i}|\vec{q}_{\rm true,1...6})$ is modeled as a second order polynomial:

$$f_{\rm large}(\vec{x_i}|\vec{q}_{\rm true,1...6}) = q_{\rm true,1} + q_{\rm true,2}\, x_i + q_{\rm true,3}\, y_i + q_{\rm true,4}\, x_i^2 + q_{\rm true,5}\, x_i\, y_i + q_{\rm true,6}\, y_i^2 \quad .$$

The small-scale instrument response, which is constructed from sine and cosine contributions, is superimposed on this large-scale instrument response. The small-scale instrument response $f_{\rm small}(\vec{x_i}|\vec{q}_{\rm true,7...260})$ is modeled as

$$\begin{aligned} f_{\rm small}(\vec{x_i}|\vec{q}_{\rm true,7...260}) &= \sum_{a=0}^{6}\sum_{b=0}^{a} \left[q_{\rm true,7+4b}\cos(k_x\, x_i) + q_{\rm true,8+4b}\sin(k_x\, x_i)\right] \\ &\quad \times \left[q_{\rm true,9+4b}\cos(k_y\, y_i) + q_{\rm true,10+4b}\sin(k_y\, y_i)\right] \quad , \end{aligned}$$

where

$$\begin{aligned} k_x &= \frac{a\,\pi}{X} \quad , \\ k_y &= \frac{b\,\pi}{Y} \quad , \end{aligned}$$

with the physical focal plane dimensions X and Y. In total, the instrument response model is parameterized with 260 parameters; an example can be seen in Figure 1(right). It is this instrument response that we try and recover with the self-calibration procedure. Our final assumption in these simulations is that the instrument response is temporally stable.

2.3. The Complete Survey

In this work we are interested in simulating complete surveys, in order to identify the crucial characteristics of survey strategies that allows for the relative instrument response model to be accurately constrained from the resulting dataset. We therefore apply the single exposure procedure introduced in the previous section for each pointing specified in a defined survey strategy. The resultant source measurements are collaged into a survey wide dataset.

3. Self-Calibrating the Survey Wide Dataset

We self-calibrate the dataset generated in the survey simulations to recover the true instrument response applied and the true source fluxes. This self-calibration procedure has been successfully applied to ground based imaging surveys, such as the Sloan Digital Sky Survey (Padmanabhan et al. 2008)[2]. This iterative procedure comprises two steps: (1) a refinement of the source flux estimates based on the latest instrument response model and (2) a refinement of the instrument response model based on the updated source flux estimates. These steps are iterated until the system converges, or until it is clear that the system will not converge. There is a degeneracy in the problem, as both the true instrument

[2]Here this procedure is dubbed "uber-calibration."

response and the true source magnitudes are unknown. It is therefore only possible to calibrate the *relative* instrument response and the *relative* source fluxes. It is not possible to know, for example, if the sources are all fainter or if the instrument response is uniformly lower. This degeneracy can be broken through observations of standard absolute sources.

3.1. Fitted Measurement Model

To complicate the simulations, we use the self-calibration procedure to fit a model that is *incomplete* in two ways. Firstly, the *fitted* instrument response is modeled as an eighth order polynomial, and not the second order polynomial superimposed with sine and cosine contributions used to model the *true* instrument response. Secondly, the assumed measurement uncertainty variances do not include the additional random measurement error ϵ_i introduced in Subsection 2.2.2. The incomplete measurement model is

$$c_i = f(\vec{x_i}|\vec{q})\, s_k + e_i \quad ,$$

where c_i is the recorded count rate, $f(\vec{x_i}|\vec{q})$ is the fitted instrument response model at a focal plane position $\vec{x}_i$, $\vec{q}$ is a vector parameterizing the eighth order polynomial instrument response model, s_k is the model source flux estimate and the error e_i is drawn from the Normal Distribution $N(e|0, {\sigma_i}^2)$, such that

$$\sigma_i^2 = \alpha^2 + \eta^2\, c_i^2 \quad ,$$

where α and η are the parameters set by the instruments 10σ and saturation limits. The ϵ_i error contribution is intentionally not included in order to simulate systematic problems with the instrument noise model.

3.2. Step 1: Source Flux Refinement

The sources are considered individually in the first step of the self-calibration procedure; their flux estimates are refined based on the latest fitted instrument response parameters $\vec{q}$. An error function χ_k^2 for all the measurements i of a source k ($i \in \mathcal{O}(k)$) is constructed:

$$\chi_k^2 = \sum_{i \in \mathcal{O}(k)} \frac{(c_i - f_i(\vec{x}_i|\vec{q})\, s_k)^2}{{\sigma_i}^2} \quad ,$$

where c_i are the measured count rates, $f(\vec{x}_i|\vec{q})$ is the fitted instrument response model at a focal plane position $\vec{x}_i$ and σ_i is the assumed noise model. A new estimate of the model source flux s_k' is then found by minimizing the error function with respect to the old model source flux s_k:

$$\frac{d\chi_k^2}{ds_k} = \sum_{i \in \mathcal{O}(k)} \frac{-2 f_i(\vec{x}_i|\vec{q})\,(c_i - f_i(\vec{x}_i|\vec{q})\, s_k')}{{\sigma_i}^2} = 0 \quad ,$$

$$s_k' \leftarrow \left[\sum_{i \in \mathcal{O}(k)} \frac{f_i(\vec{x}_i|\vec{q})^2}{{\sigma_i}^2}\right]^{-1} \left[\sum_{i \in \mathcal{O}(k)} \frac{f_i(\vec{x}_i|\vec{q})\, c_i}{{\sigma_i}^2}\right] \quad .$$

The standard uncertainty variance on the new source flux estimate s_k' is given by

$$\sigma_k'^2 = \left[\sum_{i \in \mathcal{O}(k)} \frac{f_i(\vec{x}_i|\vec{q})^2}{{\sigma_i}^2}\right] \quad .$$

3.3. Step 2: Instrument Response Refinement

The instrument response parameters can now be refined with the latest source flux estimates. A error function for all the measurements of all the sources is constructed

$$\chi^2 = \sum_k \chi_k'^2 \quad ,$$

where

$$\chi_k'^2 = \sum_{i \in \mathcal{O}(k)} \frac{(c_i - f_i(\vec{x_i}|\vec{q})\, s_k')^2}{{\sigma_i}^2} \quad .$$

Recall that the fitted instrument response $f_i(\vec{x_i}|\vec{q})$ is modeled as an eight order polynomial. This can be expressed as

$$f_i(\vec{x_i}|\vec{q}) = \sum_{l=1}^{L} q_l\, g_l(\vec{x_i}) \quad ,$$

where $L = 45$ in this case. The total error function χ^2 can be rewritten as

$$\chi^2 = \sum_k \sum_{i \in \mathcal{O}(k)} \frac{(c_i - s_k' \sum_{l=1}^{L} q_l g_l(\vec{x_i}))^2}{{\sigma_i}^2} \quad .$$

To refine the instrument response model fit, this error function is minimized with respect to the instrument response model parameters q_l

$$\frac{d\chi^2}{dq_l} = \sum_k \sum_{i \in \mathcal{O}(k)} \frac{-2 g_l(\vec{x_i}) s_k' (c_i - s_k' \sum_{l'=1}^{L'} q_{l'}' g_{l'}(\vec{x_i}))}{{\sigma_i}^2} = 0 \quad ,$$

$$\sum_k \sum_{i \in \mathcal{O}(k)} \frac{g_l(\vec{x_i}) s_k' c_i}{{\sigma_i}^2} = \sum_k \sum_{i \in \mathcal{O}(k)} \frac{g_l(\vec{x_i}) s_k'^2 \sum_{l'=1}^{L'} q_{l'}' g_{l'}(\vec{x_i})}{{\sigma_i}^2} \quad .$$

It is now simpler to proceed in matrix notation. The following substitutions can be made

$$b_l = \sum_k \sum_{i \in \mathcal{O}(k)} \frac{g_l(\vec{x_i}) s_k' c_i}{\sigma_i^2} \quad , \tag{3}$$

$$G_{ll'} = \sum_k \sum_{i \in \mathcal{O}(k)} \frac{s_k'^2}{\sigma_i^2} g_l(x_i) g_{l'}(x_i) \quad . \tag{4}$$

The matrix equation is then

$$\vec{b} = G \cdot \vec{q'} \quad .$$

The refined instrument response parameters are then found by

$$\vec{q'} \leftarrow G^{-1} \cdot \vec{b} \quad .$$

These two steps are iterated until the solution converges to a final fit of the instrument response $f_{\rm fit}(\vec{x}|\vec{q_{\rm fit}})$ and the source fluxes $s_{k,\rm fit}$, or until it is clear that a solution will not be found.

4. Metrics

To assess the performance of the self-calibration procedure with different survey strategies, it is necessary to quantify the quality of the final fitted solution. To do this we defined three quantities. The first is the root-mean-squared (RMS) error $S_{\rm RMS}$ in the final fitted source fluxes $s_{k,\rm fit}$ compared to the true source fluxes $s_{k,\rm true}$ for all the K sources:

$$S_{\rm RMS} = \sqrt{\frac{1}{K}\sum_{k}^{K}\left(\frac{s_{k,\rm fit} - s_{k,\rm true}}{s_{k,\rm true}}\right)^2} \quad . \tag{5}$$

The other two metrics, called "badnesses", are defined as the RMS error between the final fitted instrument response and a reference instrument response sampled on a regular 500×500 grid across the focal plane. For the "True Badness" $B_{\rm true}$, the *fitted* instrument response $f_{\rm fit}(\vec{x}|\vec{q_{\rm fit}})$ is compared to the *true* instrument response $f_{\rm true}(\vec{x}|\vec{q_{\rm true}})$ at the J sample points

$$B_{\rm true} = \sqrt{\frac{1}{J}\sum_{j}^{J}\left(\frac{f_{\rm fit}(\vec{x_j}|\vec{q_{\rm fit}}) - f_{\rm true}(\vec{x_j}|\vec{q_{\rm true}})}{f_{\rm true}(\vec{x_j}|\vec{q_{\rm true}})}\right)^2} \quad . \tag{6}$$

The "Best-in-Basis Badness" $B_{\rm best}$ compares the *fitted* instrument response $f_{\rm fit}(\vec{x_j}|\vec{q_{\rm fit}})$ to the *best instrument response fit possible* $f_{\rm best}(\vec{x_j}|\vec{q_{\rm best}})$ with the basis used to describe the fitted model (in this case an eight order polynomial) at the J sample points

$$B_{\rm best} = \sqrt{\frac{1}{J}\sum_{j}^{J}\left(\frac{f_{\rm fit}(\vec{x_j}|\vec{q_{\rm fit}}) - f_{\rm best}(\vec{x_j}|\vec{q_{\rm best}})}{f_{\rm best}(\vec{x_j}|\vec{q_{\rm best}})}\right)^2} \quad . \tag{7}$$

The badnesses provide a more complete description of the self-calibration performance than the RMS error on the fitted sources' fluxes, as the RMS source error only applies to the bright sources within the survey selected for the self-calibration procedure.

5. The Simple Survey Strategies

6. Discussion

In this paper, we have considered the optimization of survey strategies for calibrating the relative photometric response of an instrument, but we feel there are many more calibration parameters that can be constrained for this method. For example, the optical distortion of an instrument could also be constrained with such a method, although we concede that the properties of a survey strategy that makes them good for one calibration, may not be the same as that for another; ultimately a trade-off would need to be performed.

7. Acknowledgments

We are grateful to

REFERENCES

Padmanabhan, N., Schlegel, D. J., Finkbeiner, D. P., Barentine, J. C., Blanton, M. R., Brewington, H. J., Gunn, J. E., Harvanek, M., Hogg, D. W., Ivezić, Ž., Johnston, D., Kent, S. M., Kleinman, S. J., Knapp, G. R., Krzesinski, J., Long, D., Neilsen, Jr., E. H., Nitta, A., Loomis, C., Lupton, R. H., Roweis, S., Snedden, S. A., Strauss, M. A., & Tucker, D. L., An Improved Photometric Calibration of the Sloan Digital Sky Survey Imaging Data, 2008, ApJ, 674, 1217

Windhorst, R. A., Cohen, S. H., Hathi, N. P., McCarthy, P. J., Ryan, Jr., R. E., Yan, H., Baldry, I. K., Driver, S. P., Frogel, J. A., Hill, D. T., Kelvin, L. S., Koekemoer, A. M., Mechtley, M., O'Connell, R. W., Robotham, A. S. G., Rutkowski, M. J., Seibert, M., Straughn, A. N.,Tuffs, R. J., Balick, B., Bond, H. E., Bushouse, H., Calzetti, D., Crockett, M., Disney, M. J., Dopita, M. A., Hall, D. N. B., Holtzman, J. A., Kaviraj, S., Kimble, R. A., MacKenty, J. W., Mutchler, M., Paresce, F., Saha, A., Silk, J. I., Trauger, J. T., Walker, A. R., Whitmore, B. C., Young, E. T., The Hubble Space Telescope Wide Field Camera 3 Early Release Science Data: Panchromatic Faint Object Counts for 0.2-2 μm Wavelength, 2011, XX.

This manuscript was prepared with the AAS LaTeX macros v5.2.

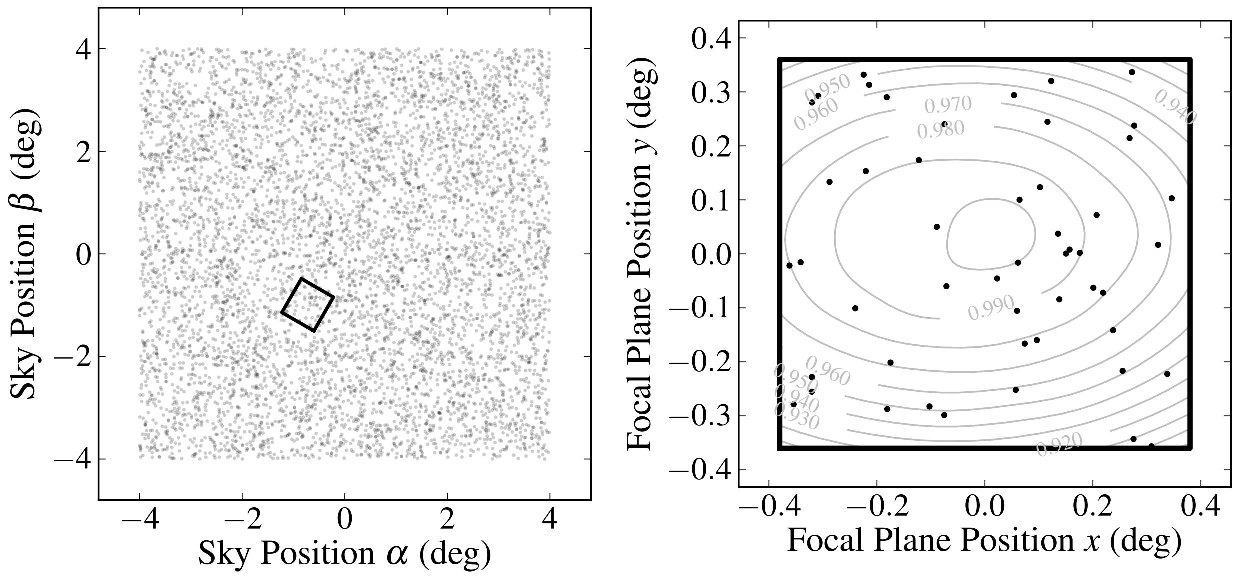

Fig. 1.— A single exposure of the synthetic sky. Left: A plot of the bright sources within the synthetic sky used in the self-calibration procedure with the focal plane footprint overlaid. Right: The resultant distribution of the sources on the instrument's focal plane. The *true* instrument model $f_{\rm true}(\vec{x}_i|\vec{q}_{\rm true})$ is shown as contours.

Table 1. A summary of the tuneable parameters in these simulations and their fiducial values.

Parameter	Fiducial Value
Source Density – Eqn. 1 ($\deg^{-2}$)	$a = -13.05, b = 1.25, c = -0.02$
Survey Area ($\deg^{2}$)	8×8
Source Density ($\deg^{-2}$)	$d = 100$
Saturation Limit (mag)	$m_{\rm min} = 17$
10σ Detection Limit (mag)	$m_{\rm max} = 22$
Field-of-View ($\deg^{2}$)	0.76×0.72
Noise Model – Eqn. 2	$\alpha = 0.1585$, $\eta = 0.0017$, $\epsilon_{\rm max} = 1.0$
Fitted Instrument Response Model	$8^{\rm th}$ order polynomial

Table 2. Sample table taken from ?

POS	chip	ID	X	Y	RA	DEC	IAU$\pm$ δ IAU	IAP1$\pm$ δ IAP1	IAP2 $\pm$ δ IAP2	star	E	Comment
0	2	1	1370.99	57.35	6.651120	17.131149	21.344$\pm$0.006	2 4.385$\pm$0.016	23.528$\pm$0.013	0.0	9	-
0	2	2	1476.62	8.03	6.651480	17.129572	21.641$\pm$0.005	2 3.141$\pm$0.007	22.007$\pm$0.004	0.0	9	-
0	2	3	1079.62	28.92	6.652430	17.135000	23.953$\pm$0.030	2 4.890$\pm$0.023	24.240$\pm$0.023	0.0	-	-
0	2	4	114.58	21.22	6.655560	17.148020	23.801$\pm$0.025	2 5.039$\pm$0.026	24.112$\pm$0.021	0.0	-	-
0	2	5	46.78	19.46	6.655800	17.148932	23.012$\pm$0.012	2 3.924$\pm$0.012	23.282$\pm$0.011	0.0	-	-
0	2	6	1441.84	16.16	6.651480	17.130072	24.393$\pm$0.045	2 6.099$\pm$0.062	25.119$\pm$0.049	0.0	-	-
0	2	7	205.43	3.96	6.655520	17.146742	24.424$\pm$0.032	2 5.028$\pm$0.025	24.597$\pm$0.027	0.0	-	-
0	2	8	1321.63	9.76	6.651950	17.131672	22.189$\pm$0.011	2 4.743$\pm$0.021	23.298$\pm$0.011	0.0	4	edge

Note. — Table 2 is published in its entirety in the electronic edition of the *Astrophysical Journal*. A portion is shown here for guidance regarding its form and content.

[a]Sample footnote for table 2 that was generated with the deluxetable environment

[b]Another sample footnote for table 2

Table 3. Literature Data for Program Stars

Star	V	b−y	m_1	c_1	ref	T_{eff}	log g	v_{turb}	[Fe/H]	ref
HD 97	9.7	0.51	0.15	0.35	2	···	···	···	−1.50	2
						5015	···	···	−1.50	10
HD 2665	7.7	0.54	0.09	0.34	2	···	···	···	−2.30	2
						5000	2.50	2.4	−1.99	5
						5120	3.00	2.0	−1.69	7
						4980	···	···	−2.05	10
HD 4306	9.0	0.52	0.05	0.35	20, 2	···	···	···	−2.70	2
						5000	1.75	2.0	−2.70	13
						5000	1.50	1.8	−2.65	14
						4950	2.10	2.0	−2.92	8
						5000	2.25	2.0	−2.83	18
						···	···	···	−2.80	21
						4930	···	···	−2.45	10
HD 5426	9.6	0.50	0.08	0.34	2	···	···	···	−2.30	2
HD 6755	7.7	0.49	0.12	0.28	20, 2	···	···	···	−1.70	2
						5200	2.50	2.4	−1.56	5
						5260	3.00	2.7	−1.67	7
						···	···	···	−1.58	21
						5200	···	···	−1.80	10
						4600	···	···	−2.75	10
HD 94028	8.2	0.34	0.08	0.25	20	5795	4.00	···	−1.70	22

Table 3—Continued

Star	V	b−y	m_1	c_1	ref	T_{eff}	log g	v_{turb}	[Fe/H]	ref
						5860	···	···	−1.70	4
						5910	3.80	···	−1.76	15
						5800	···	···	−1.67	17
						5902	···	···	−1.50	11
						5900	···	···	−1.57	3
						···	···	···	−1.32	21
HD 97916	9.2	0.29	0.10	0.41	20	6125	4.00	···	−1.10	22
						6160	···	···	−1.39	3
						6240	3.70	···	−1.28	15
						5950	···	···	−1.50	17
						6204	···	···	−1.36	11
This is a cut-in head										
+26°2606	9.7	0.34	0.05	0.28	20,11	5980	···	···	< −2.20	19
						5950	···	···	−2.89	24
+26°3578	9.4	0.31	0.05	0.37	20,11	5830	···	···	−2.60	4
						5800	···	···	−2.62	17
						6177	···	···	−2.51	11
						6000	3.25	···	−2.20	22
						6140	3.50	···	−2.57	15

Table 3—Continued

Star	V	b−y	m_1	c_1	ref	T_{eff}	log g	v_{turb}	[Fe/H]	ref
+30°2611	9.2	0.82	0.33	0.55	2	⋯	⋯	⋯	−1.70	2
						4400	1.80	⋯	−1.70	12
						4400	0.90	1.7	−1.20	14
						4260	⋯	⋯	−1.55	10
+37°1458	8.9	0.44	0.07	0.22	20,11	5296	⋯	⋯	−2.39	11
						5420	⋯	⋯	−2.43	3
+58°1218	10.0	0.51	0.03	0.36	2	⋯	⋯	⋯	−2.80	2
						5000	1.10	2.2	−2.71	14
						5000	2.20	1.8	−2.46	5
						4980	⋯	⋯	−2.55	10
+72°0094	10.2	0.31	0.09	0.26	12	6160	⋯	⋯	−1.80	19
I'm a side head:										
G5–36	10.8	0.40	0.07	0.28	20	⋯	⋯	⋯	−1.19	21
G18–54	10.7	0.37	0.08	0.28	20	⋯	⋯	⋯	−1.34	21
G20–08	9.9	0.36	0.05	0.25	20,11	5849	⋯	⋯	−2.59	11
						⋯	⋯	⋯	−2.03	21
G20–15	10.6	0.45	0.03	0.27	20,11	5657	⋯	⋯	−2.00	11
						6020	⋯	⋯	−1.56	3
						⋯	⋯	⋯	−1.58	21
G21–22	10.7	0.38	0.07	0.27	20,11	⋯	⋯	⋯	−1.23	21
G24–03	10.5	0.36	0.06	0.27	20,11	5866	⋯	⋯	−1.78	11

Table 3—Continued

Star	V	b−y	m_1	c_1	ref	T_{eff}	log g	v_{turb}	[Fe/H]	ref
						···	···	···	−1.70	21
G30–52	8.6	0.50	0.25	0.27	11	4757	···	···	−2.12	11
						4880	···	···	−2.14	3
G33–09	10.6	0.41	0.10	0.28	20	5575	···	···	−1.48	11
G66–22	10.5	0.46	0.16	0.28	11	5060	···	···	−1.77	3
						···	···	···	−1.04	21
G90–03	10.4	0.37	0.04	0.29	20	···	···	···	−2.01	21
LP 608–62[a]	10.5	0.30	0.07	0.35	11	6250	···	···	−2.70	4

[a]Star LP 608–62 is also known as BD+1°2341p. We will make this footnote extra long so that it extends over two lines.

References. — (1) Barbuy, Spite, & Spite 1985; (2) Bond 1980; (3) Carbon et al. 1987; (4) Hobbs & Duncan 1987; (5) Gilroy et al. 1988: (6) Gratton & Ortolani 1986; (7) Gratton & Sneden 1987; (8) Gratton & Sneden (1988); (9) Gratton & Sneden 1991; (10) Kraft et al. 1982; (11) LCL, or Laird, 1990; (12) Leep & Wallerstein 1981; (13) Luck & Bond 1981; (14) Luck & Bond 1985; (15) Magain 1987; (16) Magain 1989; (17) Peterson 1981; (18) Peterson, Kurucz, & Carney 1990; (19) RMB; (20) Schuster & Nissen 1988; (21) Schuster & Nissen 1989b; (22) Spite

et al. 1984; (23) Spite & Spite 1986; (24) Hobbs & Thorburn 1991; (25) Hobbs et al. 1991; (26) Olsen 1983.